

## Modeling plasmonic scattering combined with thin-film optics

This article has been downloaded from IOPscience. Please scroll down to see the full text article.

2011 Nanotechnology 22 025204

(<http://iopscience.iop.org/0957-4484/22/2/025204>)

View [the table of contents for this issue](#), or go to the [journal homepage](#) for more

Download details:

IP Address: 212.235.187.43

The article was downloaded on 07/12/2010 at 15:24

Please note that [terms and conditions apply](#).

# Modeling plasmonic scattering combined with thin-film optics

M Schmid<sup>1,2</sup>, R Klenk<sup>2</sup>, M Ch Lux-Steiner<sup>2</sup>, M Topič<sup>1</sup> and J Krč<sup>1</sup>

<sup>1</sup> Faculty of Electrical Engineering, University of Ljubljana, Tržaška 25, 1000 Ljubljana, Slovenia

<sup>2</sup> Institute for Heterogeneous Materials Systems, Helmholtz-Zentrum Berlin, Hahn-Meitner-Platz 1, 14109 Berlin, Germany

E-mail: [martina.schmid@helmholtz-berlin.de](mailto:martina.schmid@helmholtz-berlin.de)

Received 1 September 2010, in final form 26 October 2010

Published 7 December 2010

Online at [stacks.iop.org/Nano/22/025204](http://stacks.iop.org/Nano/22/025204)

## Abstract

Plasmonic scattering from metal nanostructures presents a promising concept for improving the conversion efficiency of solar cells. The determination of optimal nanostructures and their position within the solar cell is crucial to boost the efficiency. Therefore we established a one-dimensional optical model combining plasmonic scattering and thin-film optics to simulate optical properties of thin-film solar cells including metal nanoparticles. Scattering models based on dipole oscillations and Mie theory are presented and their integration in thin-film semi-coherent optical descriptions is explained. A plasmonic layer is introduced in the thin-film structure to simulate scattering properties as well as parasitic absorption in the metal nanoparticles. A proof of modeling concept is given for the case of metal-island grown silver nanoparticles on glass and ZnO:Al/glass substrates. Using simulations a promising application of the nanoparticle integration is shown for the case of CuGaSe<sub>2</sub> solar cells.

(Some figures in this article are in colour only in the electronic version)

## 1. Introduction

Nanostructures are one of the principal ideas for novel concepts in photovoltaic devices [1, 2]. Plasmonic scattering from metal nanostructures has gained attention in various fields like evanescent-wave microscopy [3], surface enhanced Raman scattering [4] and other optoelectronic applications [5, 6]. In photovoltaic devices plasmonic scattering is intended to enhance the absorption in absorber layers, enabling their thickness reduction. Absorption enhancement from integration of metal nanoparticles has been studied experimentally in different types of solar cells like amorphous silicon [7–10], organic [11] and dye-sensitized cells. The latter applications use the effect of localized surface plasmon resonance occurring at metal nanoparticles. So far, modeling has addressed aspects of particle composition [12], size, shape and dielectric environment [13–16]. Optical modeling of complete solar cell structures including nanoparticles, however, is of great interest.

In this paper we present an optical model that combines scattering and absorption from nanoparticles with the propagation of light in a multi-layer thin-film optical system. Mie theory is used to calculate absorption and scattering

cross sections of metal nanoparticles [17]. The angular power distribution of the light scattered at the particles is determined by using a dipole model approach [18]. For thin-film optics a semi-coherent optical modeling code is employed [19]. To represent scattering and absorption properties of integrated metal nanoparticles a plasmonic layer is introduced into the solar cell structures. This extended optical model is verified using examples of nanoparticles on a glass substrate (figure 1(a)) and nanoparticles on a thin layer of ZnO:Al deposited on glass (figure 1(b)). The simulation results of a complete solar cell including the nanoparticles at different locations are presented for the case of a ZnO:Al/i-ZnO/CdS/CuGaSe<sub>2</sub>/SnO<sub>2</sub>:F/glass solar cell (figures 1(c)–(e)).

## 2. Theory and developed optical models

### 2.1. Theory of localized surface plasmons

When light is incident on a metal nanoparticle the oscillating electromagnetic field of the light leads to collective oscillations of the conducting electrons (plasmonic excitations). The subsequent polarization effects and restoring forces allow for

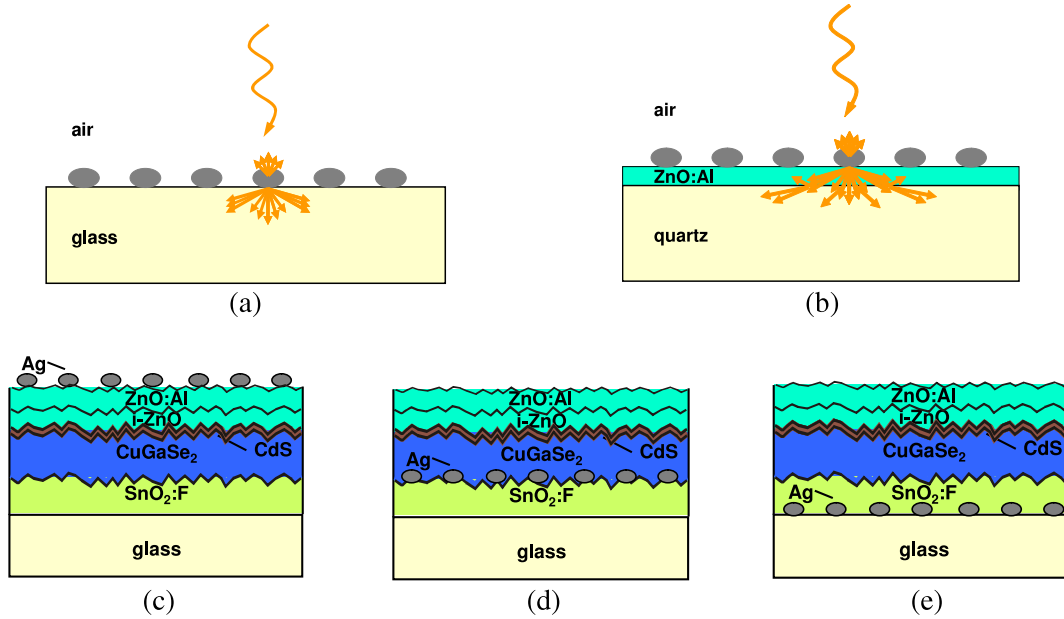


**Figure 1.** Schematics of the analyzed structures: (a) metal nanoparticles on a glass substrate, (b) nanoparticles on ZnO:Al/glass, (c)–(e) nanoparticles at different positions within an IR-transparent CuGaSe<sub>2</sub> solar cell.

the occurrence of a resonance behavior. In the wavelength region where the resonance occurs light is most efficiently scattered at the nanoparticle. At the same time also the parasitic absorption in the nanoparticle is enhanced. The beneficial feature is that light can be scattered in large angles outside the specular direction, in the so called ‘forbidden zones’. The light is trapped in the layer with higher refractive index than the neighboring media [18, 20]; this can preferentially be the absorber layer.

To describe the surface plasmon resonance the polarizability  $\alpha$  is introduced, which gives the tendency of a charge distribution (like the free electrons in a metal nanostructure) to be distorted by an external electric field. In the case of a spherical metal nanoparticle with radius  $r$  the complex function  $\alpha$  is given as [21]

$$\alpha = 4\pi r^3 \frac{\varepsilon_m - \varepsilon_d}{\varepsilon_m + 2\varepsilon_d}. \quad (1)$$

Here  $\varepsilon_m$  is the wavelength dependent complex dielectric function ( $\varepsilon_m = \varepsilon'_m + i\varepsilon''_m$ ) of the metal of the nanoparticle and  $\varepsilon_d$  is that of the surrounding dielectric. In the case of small  $\varepsilon''_m$  a pole is observed for  $\varepsilon'_m = -2\varepsilon_d$ . Since the dielectric function of a free electron metal is determined by the Drude formula as (see e.g. [22])

$$\varepsilon_m = 1 - \frac{\omega_p^2}{\omega^2 + i\omega\gamma} \quad (2)$$

( $\omega_p$  is the plasma frequency,  $\gamma$  is the damping constant) this condition corresponds to the surface plasmon resonance frequency  $\omega_{sp}$  given by

$$\omega_{sp} = \frac{\omega_p}{\sqrt{1 + 2\varepsilon_d}}. \quad (3)$$

With deviation from the spherical shape of the nanoparticle multiple resonance peaks can occur. The polarizability

(see equation (1)) changes for ellipsoidal nanoparticles with consideration of the geometric depolarization factor  $L_i$  to [22]

$$\alpha = \frac{4}{3}\pi abc \frac{\varepsilon_m - \varepsilon_d}{\varepsilon_d + L_i(\varepsilon_m - \varepsilon_d)}, \quad (4)$$

where  $a$ ,  $b$  and  $c$  are the half lengths of the main axes of the ellipsoid. For materials with the real part of the dielectric function becoming more and more negative with increasing wavelength (like in the case of silver) a shift of the dominant plasmon resonance peak towards longer wavelengths (red shift) is observed with elongation of the particles [22].

The red shift of the plasmon resonance can also occur as a result of interaction of closely adjacent nanoparticles [23]. Furthermore surrounding media with a higher refractive index cause a red shift of the plasmon resonance [15].

Most often gold, silver, copper or aluminum are considered as materials for metal nanoparticles. Among them silver stands out due to the highest scattering efficiency (80% for  $\lambda > 400$  nm according to [12]) and a resonance position around 350 nm (in air) [24]. The red shift occurs with increasing refractive index of the medium surrounding the nanoparticle. For nanoparticles at an interface the dielectric function of the surrounding medium can as an approximation be assumed as the average of the two materials ( $\varepsilon_1$  and  $\varepsilon_2$ ) at the interface [25]

$$\varepsilon_d = \varepsilon_{av} = (\varepsilon_1 + \varepsilon_2)/2. \quad (5)$$

## 2.2. Calculation of absorption and scattering cross sections of nanoparticles

Using Mie theory the total amount of scattered light and the parasitic absorption in the case of realistic particles are determined [22]. Absorption and scattering cross sections  $C_{abs}$

and  $C_{\text{sca}}$  are calculated based on the polarizability parameter defined above (see equations (1) and (4)) with  $\varepsilon_d$  from equation (5) for nanoparticles at interfaces:

$$C_{\text{abs}} = \frac{2\pi}{\lambda} \text{Im}[\alpha] \quad (6)$$

and

$$C_{\text{sca}} = \frac{1}{6\pi} \left( \frac{2\pi}{\lambda} \right)^4 |\alpha|^2. \quad (7)$$

Thus they are

$$C_{\text{abs}} \propto V \propto \begin{cases} r^3 & \text{(spherical)} \\ abc & \text{(ellipsoidal)} \end{cases} \quad (8)$$

and

$$C_{\text{sca}} \propto V^2 \propto \begin{cases} r^6 & \text{(spherical)} \\ (abc)^2 & \text{(ellipsoidal)}, \end{cases} \quad (9)$$

with the volume  $V$  being determined by either the radius  $r$  of the sphere or the half lengths  $a$ ,  $b$  and  $c$  of the main axis of the ellipsoid. The equations (6) and (7) neither depend on the angle of incident light nor on the angular distribution of radiated light. The equations show that larger nanoparticles scatter more efficiently whereas for small ones the parasitic absorption dominates. Figure 3 illustrates this behavior by showing the scattering efficiency defined as  $C_{\text{sca}}/(C_{\text{sca}} + C_{\text{abs}})$  of spherical silver nanoparticles with radii from 20 to 100 nm at the interface air–ZnO:Al. For nanoparticles with a radius of 40 nm a scattering efficiency of more than 60% above the wavelength of 500 nm can already be reached. For a scattering efficiency of over 90% a nanoparticle size of more than 80 nm radius is required. The inset in figure 3 gives the calculated scattering cross section  $C_{\text{sca}}$  for a spherical 40 nm radius silver nanoparticle. The resonance is clearly visible at  $\lambda = 400$  nm.  $C_{\text{sca}}$  reaches  $10^5$  nm<sup>2</sup> which is 20 times larger than the geometrical cross section.

When considering multiple nanoparticles in a plane, maximal absorption and scattering cross sections have to be restricted to the average area  $A_m$  corresponding to one particle (figure 4). The area  $A_m$  is defined by the density of the particles (see section 3.1). Thus, the sum of restricted  $\tilde{C}_{\text{sca}}$  and  $\tilde{C}_{\text{abs}}$  is determined as

$$\tilde{C}_{\text{sca}} + \tilde{C}_{\text{abs}} = \begin{cases} C_{\text{sca}} + C_{\text{abs}} & \text{for } C_{\text{sca}} + C_{\text{abs}} < A_m \\ A_m & \text{for } C_{\text{sca}} + C_{\text{abs}} \geq A_m, \end{cases} \quad (10)$$

while keeping the  $C_{\text{sca}}$  to  $C_{\text{abs}}$  ratio

$$\frac{\tilde{C}_{\text{sca}}}{\tilde{C}_{\text{abs}}} = \frac{C_{\text{sca}}}{C_{\text{abs}}}. \quad (11)$$

$\tilde{C}_{\text{sca}}$  and  $\tilde{C}_{\text{abs}}$  present the basis to determine the scattering level and the absorptance related to the plasmonic effect of the nanoparticles in the final thin-film optical model.

**Table 1.** Real part of the refractive index of the materials of a CuGaSe<sub>2</sub> solar cell at a wavelength of 500 nm.

	ZnO:Al	i-ZnO	CdS	CuGaSe <sub>2</sub>	SnO <sub>2</sub> :F	Glass
Real part of refractive index	1.79	2.06	2.37	3.58	2.01	1.52

### 2.3. Calculation of angular power distribution of scattered light using a dipole model approach

In a first approximation the nanoparticle or any nanostructure as mediator of plasmonic coupling can mathematically be described as a dipole oscillating at its resonance frequency. In our case we followed the approach of Mertz for calculating the angular power distribution of scattered light [18]. It is based on Lorentz' reciprocity theorem [26] stating that the description of the generation of a dipole by incident light is equal to that of the radiation of the dipole. The final equation for the calculation of the angular power distribution of the scattered light as given by Mertz [18] is

$$L_\phi(\Omega) = L_{\parallel}^{\text{s,p}}(\Omega) \sin^2 \phi + L_{\perp}^{\text{p}}(\theta) \cos^2(\phi) + \text{Re}[L_{\times}^{\text{p}}(\Omega)] \sin 2\phi. \quad (12)$$

$L_\phi(\Omega)$ ,  $L_{\parallel}^{\text{s,p}}(\Omega)$ ,  $L_{\perp}^{\text{p}}(\theta)$  and  $L_{\times}^{\text{p}}(\Omega)$  are the radiative amplitudes which are functions of the observation direction  $\Omega = (\phi, \theta)$  and depend on the field state relative to the input plane and relative to the interface (s, p and  $\parallel$ ,  $\perp$ ).  $\phi$  is the inclination of the dipole from the vertical. The derivation of equation (12) and further details can be found in [18].

Following this approach, figure 2 shows the cross sections of the calculated scattering cones of a dipole at selected interfaces, according to the structures defined in figure 1. These cross sections represent the angular power distribution in the plane of incident light. The scattering behavior is a consequence of the oscillation of the dipole in its resonance resulting from the excitation with perpendicularly incident light (regardless of front or back illumination) of a wavelength of 500 nm. The refractive indices at that wavelength are given in table 1 for the materials used in the calculations. The dipole was placed parallel to the interface—assuring most efficient excitation by perpendicularly incident light—at a distance  $d$  which is a quarter of the height of the nanoparticle considered later. A random orientation of dipoles—in horizontal and vertical direction—can in principle be included in the calculations (but was not in the examples presented here) by integrating over all possible inclination angles, see [18].

Figure 2(a) shows the situation where the metal nanoparticle is surrounded by air. The scattering is equal to the front (transmission) and the back (reflection) directions in this case. In figure 2(b) the configuration dipole at the air–glass interface is shown; a preferential scattering to the glass, which here is the medium of higher refractive index, is observed. Also the additional cones pointing to the areas of total reflection emerge (the critical angle calculated for the interface is given as a red dashed line). They become even more pronounced with higher difference in refractive indices of the neighboring materials, as can be seen for the case of an air–ZnO:Al interface in figure 2(c). Here

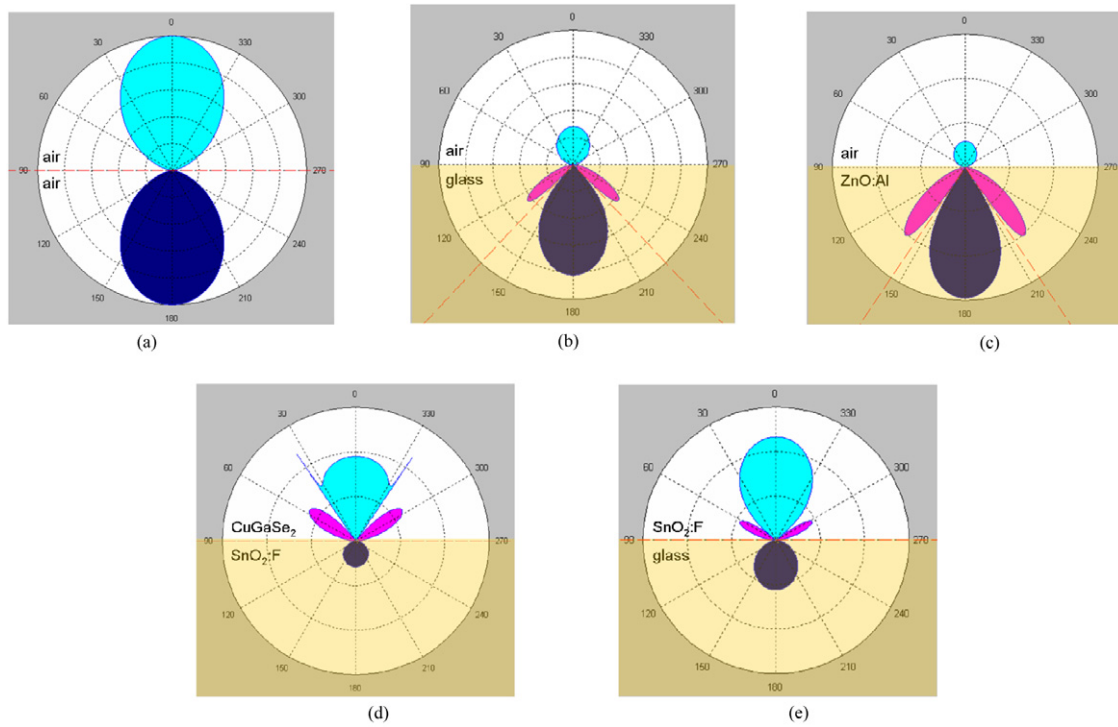


**Figure 2.** Cross section (with the incident plane) of the angular power distribution of the radiation of a dipole at the interface (a) air–air, (b) air–glass (here quartz), (c) air–ZnO:Al, (d) CuGaSe<sub>2</sub>–SnO<sub>2</sub>:F and (e) SnO<sub>2</sub>:F–glass, calculated according to equation (12). The dipole was oriented parallel to the interface, the light with a wavelength of 500 nm was perpendicularly incident (regardless of top or bottom direction).

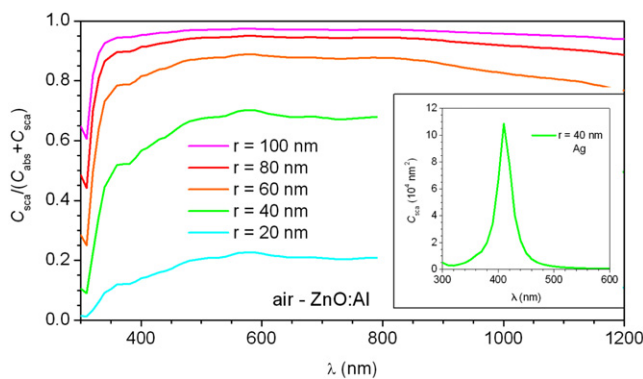


**Figure 3.** Wavelength dependent scattering efficiency  $C_{sca}/(C_{sca} + C_{abs})$  of a spherical silver nanoparticle at the interface air–ZnO:Al as a function of particle size (calculated according to Mie theory, see equations (6) and (7)).

the forward scattering is predominant and the in-coupling of light to the bottom layer highly effective. If, however, the refractive index of the bottom layer is the lower one, light is preferentially scattered backwards and the scattering behavior is inverted, according to the model. This can be seen for the examples of a dipole at the CuGaSe<sub>2</sub>–SnO<sub>2</sub>:F and at the SnO<sub>2</sub>:F–glass interfaces (figures 2(d) and (e), respectively). The calculated power distributions will present the basis to determine angular distribution functions of scattered light used as an input parameter in the thin-film optical model.

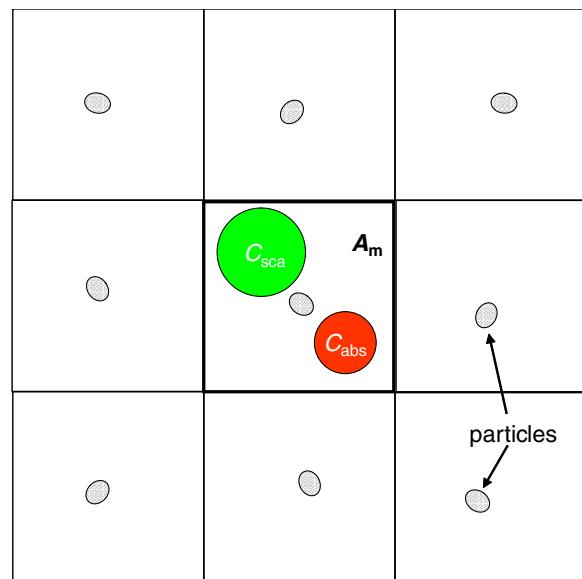


**Figure 4.** Schematic view of the wavelength dependent scattering cross section  $C_{sca}$  and absorption cross section  $C_{abs}$ , as well as the average area  $A_m$  attributed to one particle.

2.4. Modeling of localized surface plasmons in thin-film multi-layer structures

A one-dimensional semi-coherent optical model was employed [19] to describe the scattering and absorption properties in thin-film systems. Since the layer thicknesses of active devices are much smaller than the lateral extension of the

structure a one-dimensional approach is justified. In the approach, the specular non-scattered light is analyzed in terms of electromagnetic waves, so that the coherent nature of propagating light is considered. The scattered light is presented by incoherent rays with given direction and intensity. This approach of optical modeling is well established in the field of simulations of thin-film solar cells [27].

To represent the metal nanoparticles and to simulate their optical behavior inside a thin-film multi-layer system we introduce an additional layer called the plasmonic layer. It is placed at the position where the actual nanoparticles are located in the structure (inside one material or more typically at the interface of two layers). The thickness of the layer is determined by the vertical dimension of the volume occupied by the nanoparticles (height of the particles in the case of lateral placement).

Simulations showed and experiments confirmed [28] that in the wavelength region outside the plasmonic resonance peak the optical properties of the plasmonic layer can be approximated by the effective medium theory [29]. The complex refractive indices of the metal nanoparticles and that of the surrounding media are considered to determine the optical properties of the plasmonic layer in this wavelength region. In this case we have a simple optical system with an additional layer in the structure, introducing certain reflection (from the two interfaces of the layer) and absorption characteristics. A similar approach has been recently successfully implemented for nanostructured dye-sensitized solar cells [30]. In the wavelength region of the resonance peak, the plasmonic effects—light scattering and additional absorption in the nanoparticles—are applied to the layer properties in our model. Light scattering is applied to the interfaces of the plasmonic layer, by introducing (i) increased total reflection due to radiance of the nanoparticles in backward directions and (ii) diffusive properties of light in the backward (reflection) and forward (transmission) directions. Additional absorption of light in the nanoparticles at the resonance peak is considered in the model by appropriately increasing the extinction coefficient of the plasmonic layer.

The following input parameters of the thin-film model, related to the nanoparticles, are determined based on the analyses presented in previous sections:

- reflection, transmission and absorption of the nanoparticles,
- the level of diffuse light due to light scattering, represented by a haze parameter for light reflected and transmitted by the nanoparticles,
- the angular distribution function for reflected and transmitted diffuse light from the nanoparticles.

At first the absorptance related to the plasmonic effect is determined from the restricted absorption cross section  $\tilde{C}_{\text{abs}}$  (see equation (10)) and the area  $A_m$  assigned to a nanoparticle:

$$A_{\text{plasmon}} = \frac{\tilde{C}_{\text{sca}}}{A_m}. \quad (13)$$

This absorption is then added to the one that was calculated for the effective medium layer, resulting in the total absorption of the plasmonic layer  $A_{\text{tot}}$ .

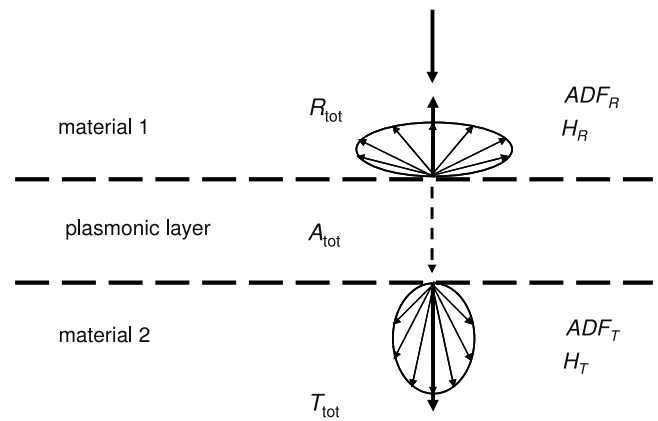


**Figure 5.** Concept of integrating plasmonic scattering and absorption in thin-film optical modeling by introducing a plasmonic layer.

Further on, the reflectance of the nanoparticles due to the scattering behavior around the resonance is determined as

$$R_{\text{plasmon}} = \frac{\tilde{C}_{\text{sca-R}}}{A_m} \quad (14)$$

where  $\tilde{C}_{\text{sca-R}}$  represents the part of the scattering cross section  $\tilde{C}_{\text{sca}}$  that corresponds to the reflected light only (backward going directions). This part can be determined from the angular power distribution obtained from the dipole calculations.

To determine the total reflectance  $R_{\text{tot}}$  from the region where the nanoparticles are located the reflectance from the plasmons and the specular reflectance calculated for the effective medium layer, considering front and back interfaces, are added in the model.

The haze level  $H_R$  related to the plasmonic scattering in backward direction is defined as

$$H_R = \frac{R_{\text{dif}}}{R_{\text{tot}}}, \quad (15)$$

where  $R_{\text{dif}}$  corresponds to the modified  $R_{\text{plasmon}}^*$ , which excludes rays reflected in specular direction ( $R_{\text{dif}} = R_{\text{plasmon}}^* < R_{\text{plasmon}}$ ).

Similarly the haze for transmitted light  $H_T$  is defined based on  $T_{\text{tot}}$  and  $T_{\text{dif}}$ , where total transmittance through the region with nanoparticles can be calculated considering the energy conservation law as  $T_{\text{tot}} = 1 - R_{\text{tot}} - A_{\text{tot}}$ .  $T_{\text{dif}}$  is determined in the same way as  $R_{\text{dif}}$ , but considering the transmitted light.

The angular distribution functions of light scattered at the nanoparticles,  $\text{ADF}_R$  and  $\text{ADF}_T$ , correspond to normalized angular power distributions obtained from the dipole calculations. Here, not only scattering in a cross sectional plane (as represented in figure 2) but scattering in the entire three-dimensional space was calculated by the Mertz approach [18] and then transferred into the 1D model [31]. In the case where nanoparticles are located at textured interfaces scattering properties of the nanoparticles and of the interfaces have to be added.

The optical situation at the plasmonic layer is shown schematically in figure 5 where the illumination is applied from the top side. The calculated reflectivity parameters ( $R_{\text{tot}}$ ,

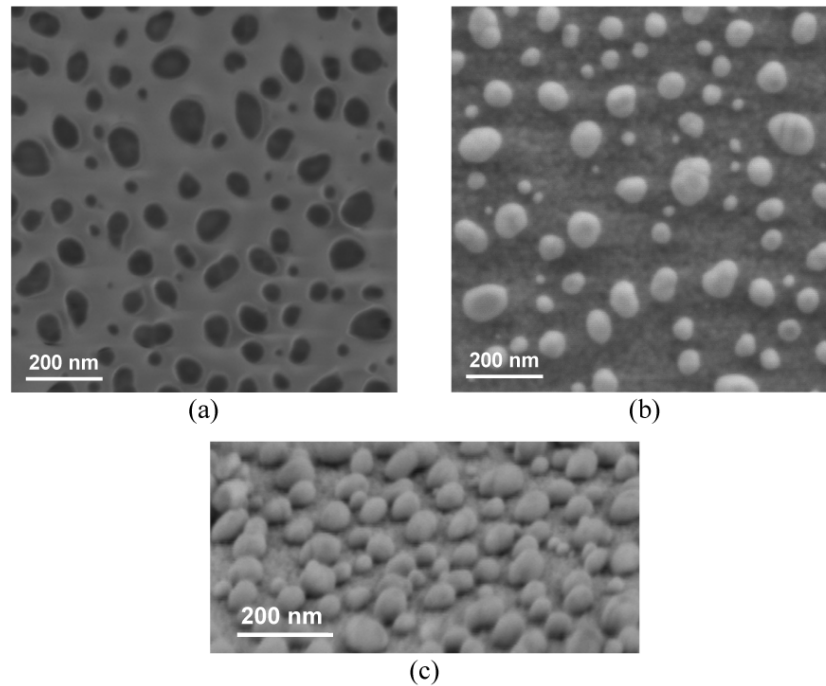


**Figure 6.** Scanning electron microscopy pictures: top views of nanoparticles produced by metal-island growth from a 12 nm silver film on (a) glass and (b) ZnO:Al/glass. (c) Side view of the nanoparticles on ZnO:Al/glass (tilting angle  $70^\circ$ ).

$H_R$  and  $ADF_R$ ) are applied to the interface where the light enters the plasmonic layer (in this case the top). Note that the simulator has to enable adaptation of the total reflectance (that is in thin-film optics calculated based on complex refractive indices of the two media forming the interface) to the required value of  $R_{tot}$  and at the same time maintain the energy conservation law at the interface. The dashed lines here indicate interfaces featuring the scattering properties related to the plasmonic effect as well as the ones of the textured interface. For the light that enters the plasmonic layer the required absorptance  $A_{tot}$  is obtained by setting the extinction coefficient of the plasmonic layer to the values that assure this absorptance. When the light enters the medium in transmission the transmittivity properties ( $H_T$  and  $ADF_T$ , while  $T_{tot}$  is already defined by  $R_{tot}$  and  $A_{tot}$ ) are applied at the second interface. In the case of a multi-layer structure light may then be reflected from rear interfaces. Thus the plasmonic layer is illuminated also from the back side and the effect of different illumination directions needs to be superimposed in the model.

### 3. Results and discussion

#### 3.1. Metal nanoparticles on substrates

Silver nanoparticles were produced by the method of metal-island growth [32]. A thin silver film was deposited by vacuum evaporation ( $p \approx 6 \times 10^{-6}$  mbar) and subsequently annealed at  $200^\circ\text{C}$  for 55 min. Nanoparticles are formed due to recrystallization and coalescence processes. The nanoparticles were grown on either glass or on a 100 nm thick ZnO:Al layer sputtered onto glass. ZnO:Al was chosen since it would correspond to the front layer of a CuGaSe<sub>2</sub> solar cell.

Figure 6 shows scanning electron microscopy (SEM) pictures of nanoparticles produced from a 12 nm thick silver film. The nanoparticle formation on bare glass (figure 6(a)) and ZnO:Al coated glass (figure 6(b)) are very similar regarding size and distribution of the nanoparticles. The difference in contrast is due to different charging of the insulating (glass) and the conducting (ZnO:Al) substrates, being in electric contact with the grounded sample holder.

The nanoparticles show an elliptical shape with average half lengths of the main axes  $a = 45$  nm and  $b = 25$  nm. Figure 6(c) gives a side view (tilting angle  $70^\circ$ ) of the nanoparticles on the ZnO:Al. From this picture it can be seen that the average half height of the nanoparticles denoted as  $c$  is similar to the parameter  $a$  (an ellipsoid with  $c = a$  was assumed in further calculations). The density of the nanoparticles and from this the average area per nanoparticle is estimated to be  $A_m = 2.5 \times 10^4$  nm<sup>2</sup>. The distance between the nanoparticles is in general larger than the average particle radius. The nanoparticles show a clear elongation and hardly any dimers are visible. Also on a larger scale only seldom connected particles were observed for this silver density. Therefore, in our calculations we consider the nanoparticles to be of elliptical shape and no interaction effects between them were taken into account. However, generally also interaction effects can be included in the properties of the plasmonic layer.

Firstly, optical properties of the sample with nanoparticles on bare glass were characterized and simulated with the developed models. In the simulations the mentioned ellipsoid parameters and  $A_m$  as derived from figure 6 were considered. Realistic optical data for silver were taken into account [33]. Optical measurements used for verification of the model were performed using a UV-vis photospectrometer with an

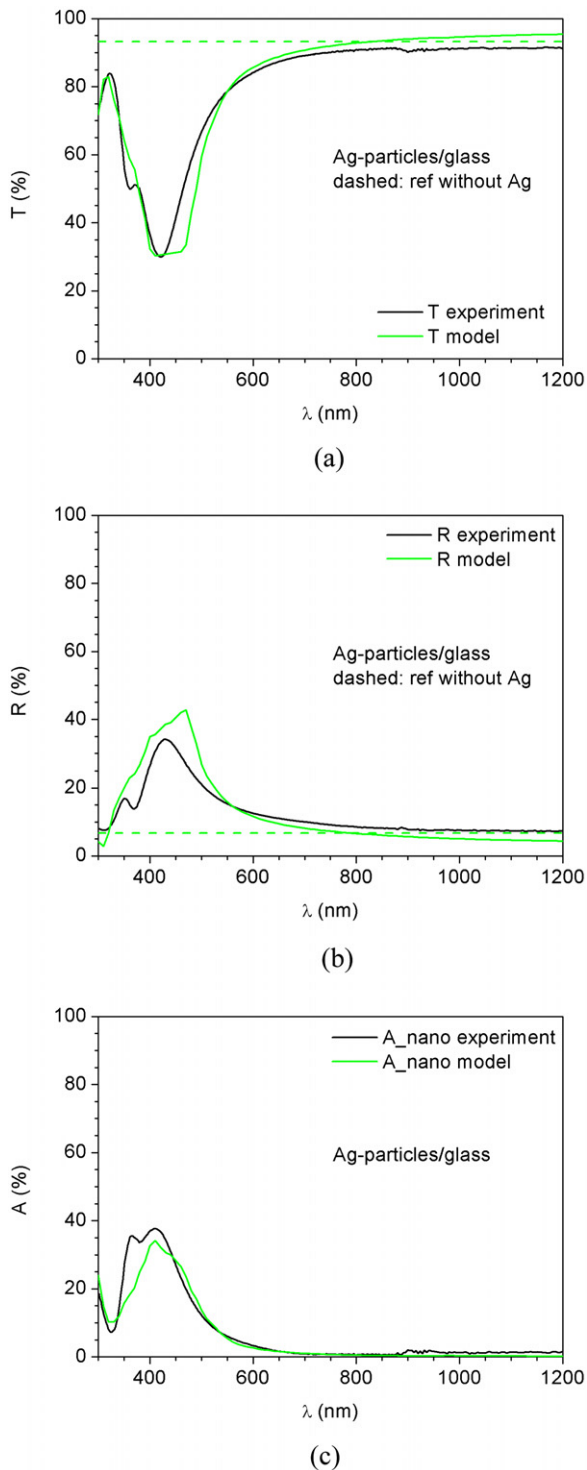


**Figure 7.** Measured and modeled (a) transmittance, (b) reflectance and (c) absorbance of small ( $a = c = 45$  nm,  $b = 25$  nm,  $A_m = 2.5 \times 10^4$  nm<sup>2</sup>) silver nanoparticles on (specifically quartz) glass; the references of a bare substrate without silver particles are plotted as dashed lines.

integrating sphere. Figures 7(a)–(c) show measured and simulated total transmission  $T$ , reflection  $R$  and absorbance  $A = 1 - R - T$  (full lines) of the sample particles on (here specifically quartz) glass illuminated from the particle side. A distinct resonance peak is observed at wavelengths

around 420 nm in both measurement and simulation. It is characterized by a minimum in transmission and a maximum in reflection and absorption. This behavior is typical for plasmonic scattering structures and is clearly different from the optical behavior of the bare substrate (dashed curves). Whereas at the resonance position the nanoparticle structure exhibits primarily scattering (and parasitic absorption) due to plasmonic effects, in the infrared the scattering of the interface including the presence of metallic silver is predominant.

The simulated transmittance, reflectance and absorbance show good general agreement with the measurements, confirming the applicability of the models. The main plasmon resonance peak position and its height are both represented correctly by the simulations. However, the second resonance peak which can be observed in measured curves at  $\lambda = 350$  nm in addition to the main peak is not present in the simulations. This second peak we assign to the elongation of the particles. Changes in optical properties due to this were not considered in the input parameters of the presented simulation.

Secondly, the modeling of plasmonic effects was transferred to the structure with nanoparticles on a 100 nm thin film of ZnO:Al on glass substrate. Measured and modeled transmittance, reflectance and absorbance are plotted in figures 8(a)–(c). The main resonance peak is here shifted to wavelengths around 480 nm due to the higher refractive index of the ZnO:Al substrate. For modeling, the parameters derived for the case of silver nanoparticles on glass were adapted to the changed interface air–ZnO:Al. The modeling curves meet the main resonance position very well again. Slight deviations in a wavelength range of 30 nm as also seen for the case of nanoparticles on glass can be explained by the fact that the same nanoparticle sizes were assumed although they may slightly differ for the case of growth on ZnO:Al. Yet, for the sake of consistency and transferability the same parameters were used throughout the modeling (ellipsoids  $a = c = 45$  nm and  $b = 25$  nm). A good general agreement of measurement and modeling is also observed in the off-resonance region. Some deviations in the wavelength range below resonance can be found and may be related to neglecting the second resonance peak in the model and to the absorption characteristics of the ZnO:Al.

### 3.2. Simulation of metal nanoparticles in the thin-film IR-transparent CuGaSe<sub>2</sub> solar cell

The simulation of optical effects of metal nanoparticles is also demonstrated on the solar cell level. One of the aims of modeling solar cells with integrated nanoparticles is to determine the best position of the nanoparticles within the structures and also to draw conclusions about appropriate nanoparticle sizes and shapes. The system investigated here was a ZnO:Al(90 nm)/i-ZnO(50 nm)/CdS(65 nm)/CuGaSe<sub>2</sub>(200 nm)/SnO<sub>2</sub>:F(90 nm)/glass solar cell that presents an option for a top cell in chalcopyrite tandems. The layer thicknesses were chosen according to the previously optically optimized structure [34] except for the CuGaSe<sub>2</sub> absorber layer thickness which was reduced from 1050 to 200 nm (this reduction of the CuGaSe<sub>2</sub> thickness decreases the native absorption from 97%

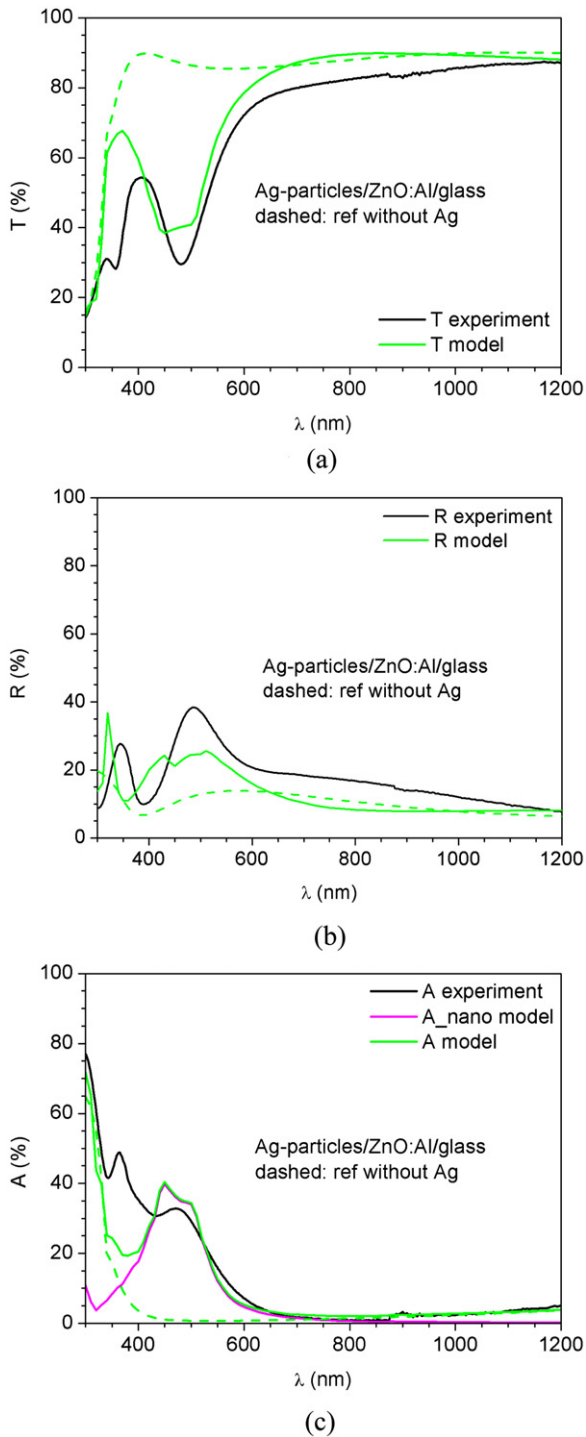


**Figure 8.** Measured and modeled (a) transmittance, (b) reflectance and (c) absorbance of small silver nanoparticles ( $a = c = 45$  nm,  $b = 25$  nm,  $A_m = 2.5 \times 10^4$  nm<sup>2</sup>) on ZnO:Al/glass substrates (absorption in particles only:  $A_{\text{nano}}$ ); the references of a 100 nm ZnO:Al film on glass without silver particles are plotted as dashed lines.

at maximum to values below 70% so that a potential absorption enhancement can be examined). In simulations realistic optical data of the layers were considered ( $E_{g-\text{CuGaSe}_2} = 1.7$  eV) [35]. Ellipsoidal nanoparticles of two different sizes were included: firstly the already mentioned dimensions  $a = c = 45$  nm,

$b = 25$  nm and  $A_m = 4 \times 10^4$  nm<sup>2</sup> ('small' particles in the following); and secondly particles with  $a = c = 75$  nm,  $b = 50$  nm and  $A_m = 4 \times 10^4$  nm<sup>2</sup> ('large' particles). In addition their position inside the solar cell structure was examined for three selected interfaces: air–ZnO:Al, CuGaSe<sub>2</sub>–SnO<sub>2</sub>:F and SnO<sub>2</sub>:F–glass (see figures 1(c)–(e)). In principle, the structure includes textured interfaces due to the polycrystalline growth of CuGaSe<sub>2</sub> and CdS. However, due to the thin CuGaSe<sub>2</sub> film the resulting root-mean-square texture is very low ( $\sigma_{\text{rms}} \sim 20$  nm) and—as simulations of the solar cell without nanoparticles indicate—the effect on the absorbance in the CuGaSe<sub>2</sub> direct band gap material is negligible. Therefore, only scattering at nanoparticles was included in these simulations. Wavelength dependent total reflectances from the structure, the parasitic absorption in the nanoparticles and absorbances in selected layers were calculated by means of the developed model. Assuming an ideal extraction of charge carriers from the CuGaSe<sub>2</sub> absorber and neglecting the contributions from the CdS layer the absorbance  $A_{\text{CuGaSe}_2}$  can be linked to the external quantum efficiency of the cell. By folding the CuGaSe<sub>2</sub> absorption with the AM1.5 solar spectrum the corresponding potential photocurrent density  $J_{\text{ph}}$  was calculated.

Initially, the small silver nanoparticles were studied on top of the IR-transparent CuGaSe<sub>2</sub> solar cell (not shown here). Due to a resonance position around  $\lambda = 480$  nm, characterized by a maximum of reflection and parasitic absorption in the nanoparticles, no absorption enhancement in the CuGaSe<sub>2</sub> layer was found for this configuration. In order to omit these losses, an insertion of the nanoparticles at the rear side is favorable. In this way also enhanced reflectivity properties of the nanoparticles around the resonance peak can be used in a beneficial way. An integration of nanoparticles within the absorber layer itself was abandoned because of electrical considerations (recombination centers).

For the two rear interfaces (CuGaSe<sub>2</sub>–SnO<sub>2</sub>:F and SnO<sub>2</sub>:F–glass) total reflection  $R_{\text{tot}}$ , absorption in the CuGaSe<sub>2</sub>  $A_{\text{CuGaSe}_2}$  and absorption in the nanoparticles  $A_{\text{nano}}$  are plotted in figure 9 for the case of small and large nanoparticles. The results are compared to the ones of the reference structure without nanoparticles, represented as dashed lines. For small nanoparticles at the CuGaSe<sub>2</sub>–SnO<sub>2</sub>:F interface (figure 9(a)) the resonance peak is shifted to  $\lambda = 740$  nm and desirably coincides with the band gap of CuGaSe<sub>2</sub>. The parasitic absorption of the nanoparticles around this wavelength does not reduce the absorption in the CuGaSe<sub>2</sub>. When considering the potential photocurrent densities an enhancement from 11.7 to 12.9 mA cm<sup>-2</sup> is observed. For the integration of the nanoparticles at the SnO<sub>2</sub>:F–glass interface (figure 9(c)) the absorption enhancement is even more pronounced and renders in total 13.2 mA cm<sup>-2</sup>. Figures 9(b) and (d) show the simulations corresponding to the structures in (a) and (c) for the large nanoparticles. Larger nanoparticles were chosen because of the higher scattering efficiency (see figure 3). The reduced parasitic absorption in the nanoparticles and a more efficient scattering lead to an absorption enhancement of 35% when placed at the CuGaSe<sub>2</sub>–SnO<sub>2</sub>:F interface. The SnO<sub>2</sub>:F–glass interface is

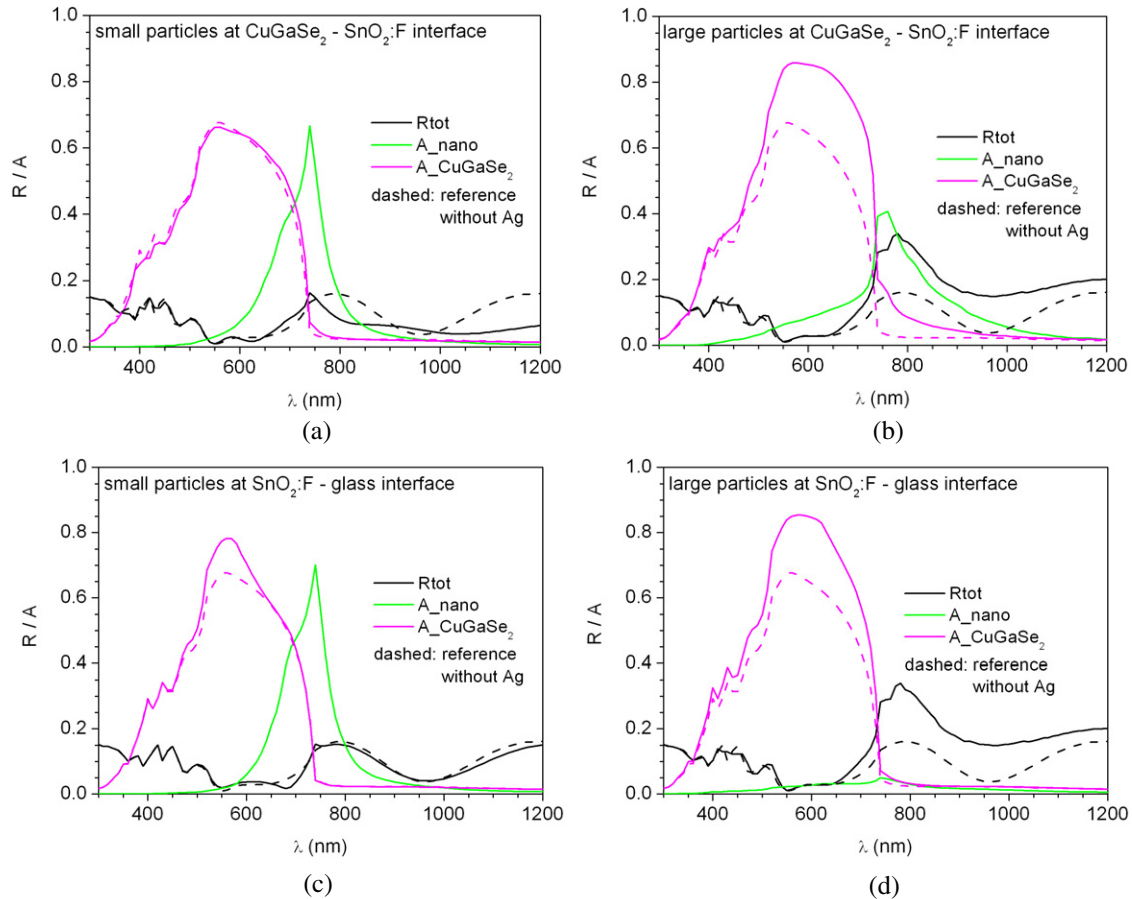


**Figure 9.** Optical modeling of a ZnO:Al/i-ZnO/CdS/CuGaSe<sub>2</sub>/SnO<sub>2</sub>:F/glass solar cell including either small ( $a = c = 45$  nm,  $b = 25$  nm) or large ( $a = c = 75$  nm,  $b = 50$  nm) silver nanoparticles. The interfaces where the particles are integrated are indicated. References for the structures without silver are shown as dashed lines.

less favorable for absorption enhancement in the CuGaSe<sub>2</sub> in the case of the large nanoparticles, possibly due to the larger distance of the nanoparticles to the absorber layer and the difficulty of coupling the scattered light through a thin layer. But still a higher absorption enhancement is found for the large nanoparticles (23% relative increase) than for the small ones (13% relative increase). The values for the potential photocurrent density  $J_{ph}$  for the configurations represented in figure 9 are summarized in table 2. As a conclusion, the rear interfaces of the CuGaSe<sub>2</sub> solar cell have proven to be beneficial for the integration of nanoparticles in order to obtain absorption enhancement from plasmonic scattering. In the case of tandem integration, a trade off between enhanced absorption in the top CuGaSe<sub>2</sub> and reduced transmittivity to the bottom CuInGaSe<sub>2</sub> cell have to be considered.

#### 4. Conclusions

We have developed an optical model combining scattering and absorption from nanoparticles with the propagation of light in a multi-layer thin-film optical system. Absorption and scattering cross sections of the nanoparticles were calculated according to Mie theory. The angular distribution of the scattered light was determined using a dipole model.

**Table 2.** Potential photocurrent density of an IR-transparent CuGaSe<sub>2</sub> solar cell with integrated silver nanoparticles, calculated from the absorption in CuGaSe<sub>2</sub> as resulting from the optical simulations shown in figure 9. Values are in mA cm<sup>-2</sup> due to a weighting with the solar spectrum in the wavelength range from 300 to 1200 nm.

$J_{ph}$ in mA cm <sup>-2</sup>	Without nanoparticles	CuGaSe <sub>2</sub> -SnO <sub>2</sub> :F	SnO <sub>2</sub> :F -glass
Small nanoparticles	11.7	12.9 (10%)	13.2 (13%)
Large nanoparticles	11.7	15.8 (35%)	14.4 (23%)

The resulting scattering and absorption parameters were integrated into thin-film optical modeling by introducing a plasmonic layer. This extended optical model showed good agreement with measurements carried out on samples of silver nanoparticles on a substrate and for nanoparticles on a thin film on substrate. It subsequently was transferred to the description of nanoparticles integrated in a ZnO:Al/i-ZnO/CdS/CuGaSe<sub>2</sub>/SnO<sub>2</sub>:F/glass solar cell with the aim of determining the best conditions in terms of nanoparticle size and position within the structure to achieve plasmonic absorption enhancement. As a result, the large nanoparticles (half lengths of the main axes of the ellipsoids  $a = c = 75$  nm and  $b = 50$  nm) inserted at the interface CuGaSe<sub>2</sub>-

SnO<sub>2</sub>:F were calculated to give a potential enhancement in photocurrent of 35%. In conclusion, our optical model enables the calculation of multi-layer thin-film structures including nanoparticles for plasmonic scattering and therefore provides a tool that assists in finding optimal structures for plasmonic absorption enhancement.

## Acknowledgments

This work was supported by the EC-projects ATHLET (No. 019670) and SOLAMON (No. 226820) as well as by the Slovenian Research Agency (program P2-0197). The contribution of M Kirkengen to the dipole calculations and the helpful discussions together with the shared knowledge of M Green's and G Conibeer's group at the UNSW, Sydney, are greatly acknowledged. The authors thank R Santbergen and T L Temple from TU Delft, The Netherlands, for useful discussions as well as M Kirsch from Helmholtz Zentrum Berlin, Germany, for ZnO-sputtering.

## References

- Conibeer G, Green M, Corkish R, Cho Y, Cho E, Jiang C, Fangsuwannarak T, Pink E, Huang Y and Puzzer T 2006 Silicon nanostructures for third generation photovoltaic solar cells *Thin Solid Films* **511/512** 654–62
- Atwater H and Polman A 2010 Plasmonics for improved photovoltaic devices *Nat. Mater.* **9** 205–13
- Oheim M, Loerke D, Chow R H and Stühmer W 1999 Evanescent-wave microscopy: a new tool to gain insight into the control of transmitter release *Phil. Trans. R. Soc. B* **354** 307–18
- Abalde-Cela S, Aldeanueva-Potel P, Mateo-Mateo C, Rodríguez-Lorenzo L, Alvarez-Puebla R A and Liz-Marzán L M 2010 Surface-enhanced Raman scattering biomedical applications of plasmonic colloidal particles *J. Roy. Soc., Interface/Roy. Soc.* **7** S435–50
- Pillai S, Catchpole K R, Trupke T, Zhang G, Zhao J and Green M a 2006 Enhanced emission from Si-based light-emitting diodes using surface plasmons *Appl. Phys. Lett.* **88** 161102
- Derkacs D, Lim S H, Matheu P, Mar W and Yu E T 2006 Improved performance of amorphous silicon solar cells via scattering from surface plasmon polaritons in nearby metallic nanoparticles *Appl. Phys. Lett.* **89** 093103
- Moulin E, Sukmanowski J, Luo P, Carius R, Royer F and Stiebig H 2008 Improved light absorption in thin-film silicon solar cells by integration of silver nanoparticles *J. Non-Cryst. Solids* **354** 2488–91
- Temple T L, Mahanama G D K, Reehal H S and Bagnall D M 2009 Influence of localized surface plasmon excitation in silver nanoparticles on the performance of silicon solar cells *Sol. Energy Mater. Sol. Cells* **93** 1978–85
- Santbergen R, Liang R and Zeman M 2010 a-Si:H solar cells with embedded silver nanoparticles *Proc. 35th IEEE PVSEC (Hawaii, June)*
- Westphalen M 2000 Metal cluster enhanced organic solar cells *Sol. Energy Mater. Sol. Cells* **61** 97–105
- Ihara M, Kanno M and Inoue S 2010 Photoabsorption-enhanced dye-sensitized solar cell by using localized surface plasmon of silver nanoparticles modified with polymer *Physica E* **42** 2867–71
- Stuart H R and Hall D G 1998 Island size effects in nanoparticle-enhanced photodetectors *Appl. Phys. Lett.* **73** 3815–7
- Catchpole K R and Polman A 2008 Design principles for particle plasmon enhanced solar cells *Appl. Phys. Lett.* **93** 191113
- Kelly K L, Coronado E, Zhao L L and Schatz G C 2003 The optical properties of metal nanoparticles: the influence of size, shape, and dielectric environment *J. Phys. Chem. B* **107** 668–77
- Beck F J, Polman A and Catchpole K R 2009 Tunable light trapping for solar cells using localized surface plasmons *J. Appl. Phys.* **105** 114310
- Kirkengen M, Bergli J and Galperin Y M 2007 Direct generation of charge carriers in c-Si solar cells due to embedded nanoparticles *J. Appl. Phys.* **102** 093713
- Mie G 1908 Beiträge zur Optik trüber Medien, speziell kolloidaler Metallösungen *Ann. Phys.* **330** 377–455
- Mertz J 2000 Radiative absorption, fluorescence, and scattering of a classical dipole near a lossless interface: a unified description *J. Opt. Soc. Am. B* **17** 1906–13
- Krc J, Smole F and Topic M 2003 Analysis of light scattering in amorphous Si:H solar cells by a one-dimensional semi-coherent optical model *Prog. Photovolt.: Res. Appl.* **11** 15–26
- Benisty H, Stanley R and Mayer M 1998 Method of source terms for dipole emission modification in modes of arbitrary planar structures *J. Opt. Soc. Am. A* **15** 1192–201
- Kreibig U and Vollmer M 1995 *Optical Properties of Metal Clusters* (Berlin: Springer)
- Bohren C F and Huffman D R 1983 *Absorption and Scattering of Light by Small Particles* (New York: Wiley)
- Khoury C G, Norton S J and Vo-dinh T 2009 Plasmonics of 3D nanoshell dimers element method *ACS Nano* **3** 2776–88
- Taneja P, Ayyub P and Chandra R 2002 Size dependence of the optical spectrum in nanocrystalline silver *Phys. Rev. B* **65** 1–6
- Xu G, Tazawa M, Jin P, Nakao S and Yoshimura K 2003 Wavelength tuning of surface plasmon resonance using dielectric layers on silver island films *Appl. Phys. Lett.* **82** 3811
- Nieto-Vesperinas M and Wolf E 1986 Generalized Stokes reciprocity relations for scattering from dielectric objects of arbitrary shape *J. Opt. Soc. Am. A* **3** 2038
- Krč J, Zeman M, Smole F and Topič M 2002 Optical modeling of a-Si:H solar cells deposited on textured glass/SnO<sub>2</sub> substrates *J. Appl. Phys.* **92** 749–55
- Schmid M 2009 *Optik der CuGaSe<sub>2</sub> Solarzelle für hocheffiziente Tandemkonzepte PhD Thesis* Freie Universität Berlin
- Ohlidal I, Navratil K and Ohlidal M 1995 Scattering of light from multilayer systems with rough boundaries *Prog. Opt.* **34** 251–334
- Topič M, Čampa A, Filipič M, Berginc M, Krašovec U O and Smole F 2010 Optical and electrical modelling and characterization of dye-sensitized solar cells *Curr. Appl. Phys.* **10** S425–30
- Krč J 2003 Analysis and modelling of thin-film optoelectronic structures based on amorphous silicon *PhD Thesis* University of Ljubljana
- Heilmann A 2003 *Polymer Films with Embedded Metal Nanoparticles* (Berlin: Springer)
- Palik E 1985 *Handbook of Optical Constants of Solids* (New York: Academic)
- Schmid M, Krč J, Klenk R, Topič M and Lux-Steiner M C 2009 Optical modeling of chalcopyrite-based tandems considering realistic layer properties *Appl. Phys. Lett.* **94** 053507
- Schmid M, Klenk R and Lux-Steiner M C 2009 Quantitative analysis of cell transparency and its implications for the design of chalcopyrite-based tandems *Sol. Energy Mater. Sol. Cells* **93** 874–8